Available online at www.sciencedirect.com
SCIENCE DIRECT
Catalysis Today 101 (2005) 163–173
CATALYSIS TODAY
www.elsevier.com/locate/cattod

Dependence of metathesis activity of Mo-methylidene sites on their location on (1 0 0) γ-Al_2O_3—a theoretical study

Jarosław Handzlik [a,*], Jan Ogonowski [a], Renata Tokarz-Sobieraj [b]

[a] *Institute of Organic Chemistry and Technology, Cracow University of Technology, ul. Warszawska 24, PL 31-155 Kraków, Poland*
[b] *Institute of Catalysis and Surface Chemistry, Polish Academy of Sciences, ul. Niezapominajek 8, PL 30-239 Kraków, Poland*

Abstract

Pathways of ethene metathesis proceeding on two Mo-methylidene sites differently located on the (1 0 0) surface of γ-Al_2O_3 are investigated with DFT calculations, applying a relatively large cluster model of alumina. Convergence of the electronic properties with respect to the cluster size is achieved for clusters as large as $Al_8O_{26}H_{28}$. It is shown that location of the active site influences its reactivity towards ethene. When the Mo-methylidene centre replaces two basic hydroxyl groups, ethene addition, leading to a trigonal bipyramidal molybdacyclobutane, is an endothermic process with relatively high activation energy. On the other hand, when only one basic OH group is replaced by the Mo centre and the molybdenum atom is also directly bonded to a bridge oxygen of the alumina surface, electron density on the Mo-methylidene moiety is reduced, comparing to the first case, and also the geometry of the site is more suitable for alkene addition. Ethene attack on this molybdenum site results in formation of a stable π-complex that can further rearrange with a low energy barrier to the trigonal bipyramidal molybdacyclobutane.

For both pathways investigated, it is predicted that rearrangement of the trigonal bipyramidal intermediate to a much more stable square pyramidal molybdacyclobutane proceeds easier than continuation of the catalytic cycle of ethene metathesis.

Keywords: Alumina; Molybdenum; Catalyst; Ethene; Metathesis; DFT; Gaussian; Molybdacyclobutane; DOS

1. Introduction

γ-Alumina is used as a support in many industrial processes, which include olefin metathesis [1,2]. A Re_2O_7/Al_2O_3 catalyst promoted with tetrabutyltin was applied in FEAST process (Further Exploitation of Advanced Shell Technology) for manufacture of α,ω-dienes by ethenolysis of cycloalkenes. Metathesis of ethene and butene to propene can be industrially carried out in liquid phase in the presence of the rhenium-alumina catalyst as well. Olefin metathesis on alumina supported molybdate catalyst is involved in the large-scale Shell Higher Olefins Process (SHOP) for converting ethene to detergent-range alkenes [1,2].

It was proposed [2] that ReO_4^- ions on alumina support react predominantly with coordinatively unsaturated Al^{3+} Lewis acid sites and with the most basic OH groups. When the Re loading increases, the neutral and more acidic hydroxyl groups are replaced, what results in relatively electron-poor rhenium centres. These centres are the precursors of the metathesis active sites, because reduced electron density on the metal facilitates alkene addition. Such explanation is strongly supported by the fact that acidity of the support favours metathesis activity of rhenium oxide catalysts [2–4]. One can expect that metathesis activity of surface Mo sites also depend on their location on the support and its properties. Indeed, there are some experimental data indicating that acidity of the support affects metathesis activity of the Mo-based catalysts [5–7]. This relationship, however, is not so well recognised as in the case of the rhenium systems. Therefore, theoretical approach seems to be helpful in investigation of the influence of the local support properties on the Mo centres reactivity.

Theoretical studies of olefin metathesis catalysed by Mo-based systems, both homogeneous [8–14] and heteroge-

* Corresponding author. Tel.: +4812 6282761; fax: +4812 6282037.
E-mail address: jhandz@usk.pk.edu.pl (J. Handzlik).

0920-5861/$ – see front matter © 2005 Elsevier B.V. All rights reserved.
doi:10.1016/j.cattod.2005.01.014

neous [15–19], confirmed the commonly accepted carbene mechanism of the process [20]. Cycloaddition of alkene to the metal-alkylidene complex, resulting in metallacyclobutane formation, is the first step of the catalytic cycle. Then, the metallacyclobutane intermediate decomposes to a new alkene molecule and the second metal-alkylidene structure. DFT investigations of model Mo-alkylidene catalysts, $Mo(NH)(CHR)(L)_2$ ($R = H$, CH_3; $L = OH$, OCH_3, OCF_3) and $Mo(O)(CH_2)(L)_2$ ($L = Cl$, OCH_3, OCF_3), confirmed that the molybdacyclobutane complexes can adopt both trigonal bipyramidal (TBP) and square pyramidal (SP) geometry [10–12,14]. According to the calculated results, the relative electron-withdrawing L ligands facilitate formation of the TBP intermediate and lower the activation barrier of the cycloaddition step [10,12,14]. These findings are consistent with experimental results concerning olefin metathesis carried out in presence of $Mo(CHR)(NAr)(OR)_2$ systems [21–23].

In the previous works, mechanism of ethene [15,16] and propene metathesis, both productive [17] and non-productive [18], was in detail investigated for molybdena–alumina system, described with simple cluster models. The next step was to consider different locations of the active sites on the carrier [19]. For the surface Mo-alkylidene complexes, the support is a ''ligand'' [24] and its local electronic properties should influence kinetics of alkene metathesis. In [19], pathways of propene addition to Mo-methylidene centres located on the (1 0 0) and (1 1 0) surfaces of γ-Al_2O_3 were compared, applying the cluster approach. In the first case, the Mo-alkylidene complex replaced basic hydroxyl groups, while in the second case more acidic hydroxyl groups were substituted. It was shown that local electronic properties of the support influence activation barriers of alkene metathesis proceeding on the Mo centres, as well as affect the relative energies of the reaction intermediates.

In the present work, pathways of ethene metathesis proceeding on two monomeric Mo-methylidene sites differently located on the (1 0 0) surface of γ-Al_2O_3 are investigated and compared. We show that position of the active centre determines both its electronic properties and some geometrical parameters that affect the kinetics of alkene metathesis. The support was represented by a larger cluster model than previously [19]. Similarly as in the earlier works [15–19], the usually suggested pseudo-tetrahedral Mo-alkylidene centre, in which Mo is bonded to the support via two oxygens and possesses the oxo spectator ligand [25–27], was taken as the model of the active site. This model can be described by the formula $Mo(O)(CH_2)$(support), where the support is considered as a bidentate ligand.

2. Computational methods

2.1. Modelling of the (1 0 0) surface of γ-Al_2O_3

Description of catalytic systems containing metal oxides and molecular or atomic adsorbate requires a fair number of approximations to allow a theoretical treatment based on models (by definition, incomplete with respect to the real systems). The preview calculations of catalytic systems [28,29] show that the local interactions of substrate with the catalyst, near the adsorption site, where the catalytic reaction is expected to happen, are well reproduced by using a cluster model. In cluster model the substrate atoms are cut out from the surface/bulk of the catalyst, i.e. the assumption of a localized interaction near the adsorption site and the neglect of the long-range interactions were introduced. The main drawback of the cluster model is the incorrect treatment of atoms at the cluster periphery [30], which manifests itself in the dependence of the calculated physical and chemical parameters on the size and geometry of the cluster. Therefore, the application of cluster model requires systematic studies where clusters of different size and shape, exhibiting different local states, are examined.

A defect spinel structure is commonly accepted for γ-Al_2O_3 [31]. Spinel has 24 cations and 32 anions in the cubic unit cell. In γ-alumina, both tetrahedral and octahedral cation positions were occupied by aluminium atoms, while oxygen atoms are closely packed. To satisfy the Al_2O_3 stoichiometry, $2\frac{2}{3}$ of the 24 cation sites should be vacant. Despite of many experimental [32,33] and theoretical [34–36] studies undertaken, there is still a controversy concerning the exact location of the vacancies. On the other hand, these vacancies were not usually taken into account during modelling the γ-Al_2O_3 surface within the cluster approach [37–39]. The exception is a very large cluster model of γ-Al_2O_3 (120 atoms) applied in semi-empirical PM3 study of alcohols chemisorption [40].

It is believed that the (1 1 0) plane of γ-Al_2O_3 is preferentially exposed, however, the (1 0 0) surface should also be taken into account [41,42]. As the experimentally determined number of metathesis sites on alumina is only a small fraction of the molybdenum atoms present [1,43], both planes can be considered. In the present work, the systematic studies of (1 0 0) surface of Al_2O_3 system are performed. The proposed clusters are cut out from the ideal γ-Al_2O_3 crystal structure [31]. Although our cluster models are quite large, they seem still too small to study the localization of the vacancies—only one cation vacancy could be included in our more advanced models and its position would have to be chosen arbitrary. To take into account the effect of structural and electronic coupling with the environment, hydrogen atoms are saturating each cluster. The number of H atoms is chosen in such a way that the whole cluster bear no charge (formal oxidation states for Al^{3+} and O^{2-} are assumed). The following sets of surface clusters, containing four aluminium atoms from the sublayer, are discussed: $Al_4O_{16}H_{20}$, $Al_6O_{22}H_{26}$, $Al_8O_{26}H_{28}$, $Al_{10}O_{30}H_{30}$, $Al_{12}O_{34}H_{32}$ (see Fig. 1). Clusters are chosen in such a way that each smaller cluster forms a subsection of the bigger one.

The electronic properties of the clusters cut out from the (1 0 0) surface are elaborated by discussing the following electronic parameters: atomic charges follow from the

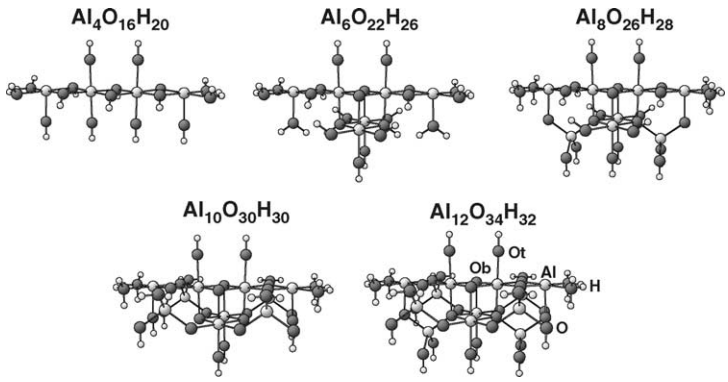

Fig. 1. Clusters used to model (1 0 0) surface of γ-Al_2O_3. The Al (O) atoms are shown as shaded (black) balls while small shaded balls refer to H atoms used to saturate oxygen atoms at the surface periphery.

Mulliken population analysis [44], Mayer bond-order indices [45], as well as distribution of populations of molecular orbitals. All electronic parameters connected with cluster convergences are evaluated with the gradient-corrected PBE functional [46].

2.2. Modelling of Mo-methylidene centres on the (1 0 0) surface of γ-Al_2O_3

As arises from the carbene mechanism [1,20], in the case of ethene metathesis, metal-methylidene complexes are involved in the process. Therefore, models of Mo-methylidene centres attached to the selected Al_8 cluster (vide infra) have been considered. In Fig. 2, two different locations of the active sites are shown. The first structure (**1a**) is analogous to that proposed previously [17,19], however, a larger cluster model of alumina is presently applied. In this model, the Mo centre replaced basic terminal hydroxyl groups bonded to octahedrally coordinated aluminium atoms (see Figs. 1 and 2) [41]. In the second structure (**1b**), the molybdenum is connected with one aluminium atom via linkage oxygen, as well as it is directly bonded to the bridge O4 atom of the support (Fig. 2). Comparing to the **1a** model, O2 atom and two terminating hydrogens from the bottom part of the alumina cluster are removed in **1b**, so the formal oxidation state of Mo is the same in both structures. The third possibility of the position of the Mo-methylidene centre, in which the molybdenum is initially bonded to both bridge O4 and O5 atoms, has also been considered. However, in this case, a four-membered ring structure with the Mo bonded to the O5 atom and the carbon atom directly connected with the Al2 atom, was obtained after the geometry optimisation. Such a structure is not a metathesis active site and it has not been further considered.

All the calculations were carried out with the GAUSSIAN 03 [47] set of programs. The hybrid B3LYP functional [48,49] was applied in the investigations of ethene metathesis. The Hay–Wadt effective core potential [50] plus double-zeta basis set (the LANL2DZ basis) was used to describe molybdenum. For C, H, O and Al the Dunning-Huzinaga full double-zeta basis set (D95) [51] was used. This basis combination is denoted here as A. Additionally, a single point energy calculations were performed using the D95(d,p) basis for C, O, Al and H, whereas Mo was described by the LANL2DZ basis set (denoted as B).

All structures of the active sites were optimised with A basis by applying the Berny algorithm and using redundant internal coordinates [52]. Only the first layer of the alumina part was allowed to be relaxed during the geometry optimisation, whereas the positions of other atoms were frozen in their crystallographic positions. In the initial structures, each terminating hydrogen was placed 0.97 Å from the oxygen, in the direction of the removed Al atom. The positions of these hydrogen atoms were also frozen.

Analysis of harmonic vibrational frequencies allowed to confirm the potential energy minima or the transition states involved in the reaction paths. The zero-point energy (ZPE) corrections are included in all the presented relative energies. These corrections are in the range of 8–17 kJ mol^{-1}. Local electronic properties of the active centres have been analysed with help of the Mulliken population analysis [44], the natural population analysis (NPA) [53,54] and the Mayer bond-order indices [45]. In this case, the B3LYP/B//B3LYP/A calculations were done.

3. Results and discussion

3.1. Electronic structure of the alumina (1 0 0) surface

Table 1 presents the fluctuations of electronic structure parameters (atomic charges and bond orders) for selected atoms from the central part of the appropriate clusters. Analyzing the charge variations at the aluminium and oxygen atoms as a function of cluster size one can conclude that the charge fluctuations stabilize for $Al_8O_{26}H_{28}$ cluster. Aluminium atoms are positively charged and their charge is close to 0.7. Oxygen centres are negatively charged and the charge on oxygen atoms coordinated with one aluminium atom is equal to −0.7. Similarly, the charge accumulated on bridging oxygen atoms (triply coordinated) converges to the value of −0.6. The Mayer bond-order indices are stabilized

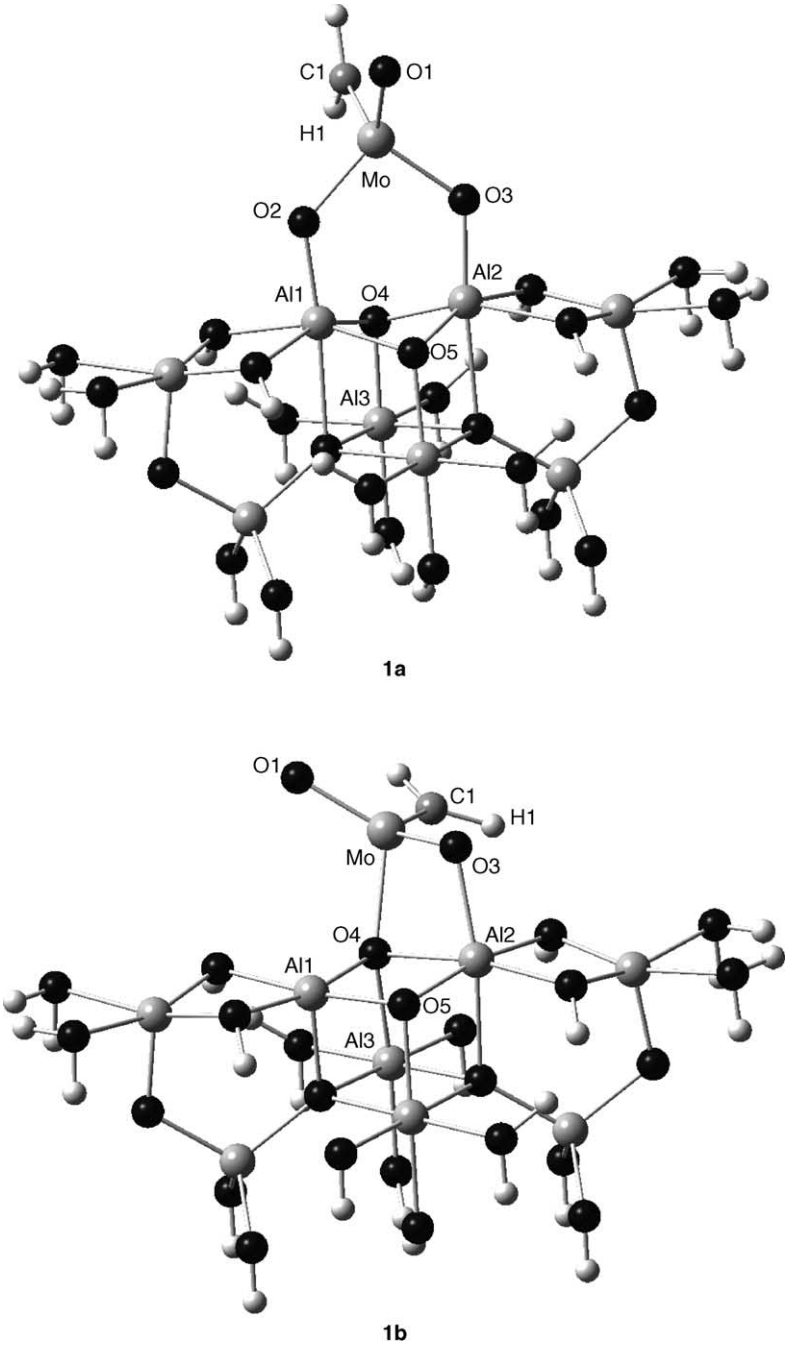

Fig. 2. Models of Mo-methylidene centres on the (1 0 0) surface of γ-Al_2O_3: Mo(O)(CH_2)($Al_8O_{26}H_{26}$) (**1a**) and Mo(O)(CH_2)($Al_8O_{25}H_{24}$) (**1b**).

on the value of 0.6, suggesting a weaker bonding than for single Al–O bonds for both types of oxygen atoms. Also the bond orders do not change starting from $Al_8O_{26}H_{28}$ cluster. Presented above results indicate that convergence in the calculated quantities is achieved with $Al_8O_{26}H_{28}$ cluster.

Another way of evaluating cluster models is to check the behavior of the HOMO energy. The negative Kohn–Sham energy, which defines the cluster ionization potential, is expected to converge with cluster size towards the work function of the extended surface system. From Table 1, one can see that the present calculations yield HOMO values which vary between −2.75 and −4.51 eV, depending on the cluster size. As before, the energy of the highest occupied orbital as well as the gap between the highest occupied and the lowest unoccupied orbitals stabilize for $Al_8O_{26}H_{28}$ cluster.

Additional information about an electronic structure of the surface clusters can be based on a characterization of their valence band region. Fig. 3 presents both the total (DOS) and the atom projected (PDOS) densities of states of $Al_6O_{22}H_{26}$, $Al_8O_{26}H_{28}$, and $Al_{12}O_{34}H_{32}$ clusters. For the sake of clarity and possibility of comparison with an

Table 1
The electronic structure parameters (atomic charges, bond-order indices), energy of HOMO orbital and the gap between the HOMO and LUMO for clusters modeling the (1 0 0) surface of γ-Al_2O_3 system

	$Al_4O_{16}H_{20}$	$Al_6O_{22}H_{26}$	$Al_8O_{26}H_{28}$	$Al_{10}O_{30}H_{30}$	$Al_{12}O_{34}H_{32}$
Charges from Mulliken population analysis					
Al	0.50	0.66	0.72	0.73	0.72
Ot	−0.40	−0.69	−0.66	−0.66	−0.65
Ob	−0.75	−0.60	−0.60	−0.60	−0.61
Mayer bond-order indices					
Al═Ot	0.83	0.68	0.58	0.58	0.58
Al–O–Al	2 × 0.54	2 × 0.62	2 × 0.59	2 × 0.60	2 × 0.59
e_{HOMO} [eV]	−2.75	−3.65	−4.44	−4.46	−4.51
$\Delta e_{HOMO-e_{LUMO}}$ [eV]	1.27	1.39	1.40	1.39	1.41

experiment, a Gaussian level broadening of 0.4 eV smooths the atoms contribution curves and the energy of the highest occupied cluster level is taken as the zero energy. Fig. 3 shows that the valence band region of Al_2O_3 system can be divided into two parts: the upper valence band between −10 and 0 eV and the lower valence in the −21 to −15 eV energy range. The valence band region yields a multi-peak structure which is described by dominantly O 2sp contributions, while aluminium contributions are smaller and confined only to the lower part of the upper valence band region. From Fig. 3 one can see that density of states for cluster containing eight aluminium ions is similar with larger cluster with 12 aluminium, specially if we consider character of molecular orbitals close to the Fermi level.

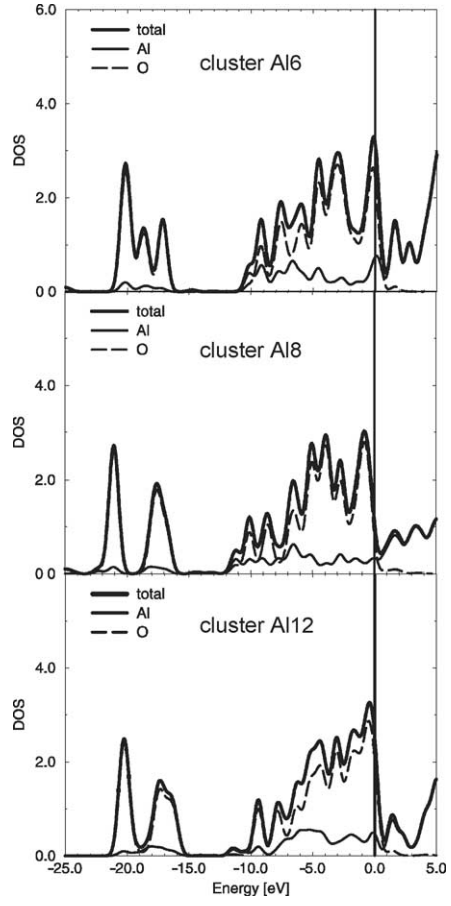

Fig. 3. Total and atom projected densities of states of the valence band region calculated for $Al_6O_{22}H_{26}$, $Al_8O_{26}H_{28}$ and $Al_{12}O_{34}H_{32}$ clusters. The energetic position of the highest occupied cluster orbital is marked by the thick vertical line.

The analysis of electronic and energetic properties of all the studied clusters allow one to conclude that $Al_8O_{26}H_{28}$ cluster is an adequate model to represent the (1 0 0) surface of γ-Al_2O_3 system, therefore the ensuing discussion is limited to this cluster.

3.2. Properties of the surface Mo-methylidene sites

The optimised structures of the four-coordinate Mo-methylidene centres **1a** and **1b** are shown in Fig. 2. The sites possess pseudo-tetrahedral geometry and are analogous to the homogeneous Schrock catalysts [21–23]. The geometry of **1a** is also very similar to the previously proposed Mo-methylidene centre on the (1 0 0) surface, where a smaller cluster model of alumina was used [17,19]. The selected geometrical parameters and bond orders for both structures are listed in Table 2. As one can see, the carbene bond is a

Table 2
Calculated geometrical parameters and bond orders (*P*) for the Mo-methylidene centres **1a** and **1b**

	1a		**1b**	
	Atomic distance (Å)	*P*	Atomic distance (Å)	*P*
Mo–C1	1.911	1.63	1.900	1.60
Mo–O1	1.735	1.92	1.731	1.95
Mo–O2	1.892	0.91	–	–
Mo–O3	1.892	0.91	1.853	1.22
Mo–O4	3.620	0.04	2.058	0.53
O2–Al1	1.802	0.78	–	–
O3–Al2	1.802	0.78	1.922	0.56
O4–Al1	1.856	0.57	1.882	0.47
O4–Al2	1.856	0.57	2.051	0.28
O4–Al3	1.855	0.65	2.001	0.29
	Angle (°)		Angle (°)	
O2–Mo–O3	98.1		–	
O4–Mo–O3	53.7		82.2	
O1–Mo–C1	104.0		107.1	
O3–Mo–C1–H1	52.9		22.7	

little shorter in **1b**, comparing to **1a**, while the Mo=O bond in both structures has very similar length and order. Larger differences are noticeable in the case of the formally single Mo–O bonds. The Mo-alkylidene complex **1a** has C_s symmetry with both Mo–O distances identical. In **1b**, the Mo–O4 bond is much longer and of half order, whereas the Mo–O3 bond is shorter than in the case of **1a** and has the order greater than 1. Consequently, in **1b**, O3 atom is more weakly bonded to Al2 than in **1a**. O4 atom in **1a** is approximately equally coordinated by three neighbouring aluminiums. This is not the case in **1b**, where the considered three bonds are of different strengths and weaker than in **1a**. What is important, the Mo=C bond in **1b** seems to be much better exposed to alkene attack than in **1a** (compare the values of the O3–Mo–C1–H1 dihedral angle—Table 2 and Fig. 2).

According to both Mulliken population analysis and NPA, a more positive charge on molybdenum and a more negative charge on the C atom are predicted in the case of the **1a** structure, comparing to **1b** (Table 3). However, the positive charge of the Mo(=O)(=CH_2) fragment of **1b** is larger than that of **1a**. This is because the basicity of the bridge O4 atom (Fig. 2) on the alumina surface is lower than the basicity of O2 and O3 if they are the terminating oxygens. Reduced electron density on the alkylidene moiety should facilitate alkene addition to the carbene bond.

In Fig. 4, isosurfaces of two molecular orbitals, the occupied one and the unoccupied one, important for reactivity of the Mo=C bond towards alkene molecule, are shown. The

Table 3
Selected charges for the Mo-methylidene centres and the π-complex

	1a		**1b**		**2b**	
	Mulliken	NPA	Mulliken	NPA	Mulliken	NPA
q(Mo)	1.37	1.63	1.31	1.55	1.10	1.35
q(C1)	−0.75	−0.71	−0.66	−0.56	−0.59	−0.44
q($MoOCH_2$)	0.47	0.69	0.56	0.81	0.46	0.80
q(C2)	–	–	–	–	−0.31	−0.41
q(C3)	–	–	–	–	−0.37	−0.41
q(C_2H_4)	–	–	–	–	0.22	0.12

occupied one (HOMO in the case of **1a**), composed mainly of d_{xz} orbital of Mo and p_z orbital of C1, is a potential electron donor towards the LUMO of alkene molecule. The acceptor orbital (LUMO in the case of **1b**), being predominantly a mixture of Mo and d orbitals, can interact with the HOMO of alkene. The shape of the LUMO of **1b** indicates that there is a preferential side for a nucleophilic attack. This side corresponds to the mentioned good geometrical exposition of the Mo=C bond to alkene addition.

The energies of the considered orbitals in **1a** are over 2 eV higher than the corresponding values for **1b**. This is the effect of higher electron withdrawing ability of the support part of the latter system. The LUMO of ethene is 4.5 eV higher than the donor orbital (HOMO) of **1a**. This value can be compared with 6.8 eV—the corresponding energy gap for **1b**. The predicted energy gap between the acceptor orbital (LUMO) of **1b** and the HOMO of ethene is 4.4 eV, while the corresponding difference

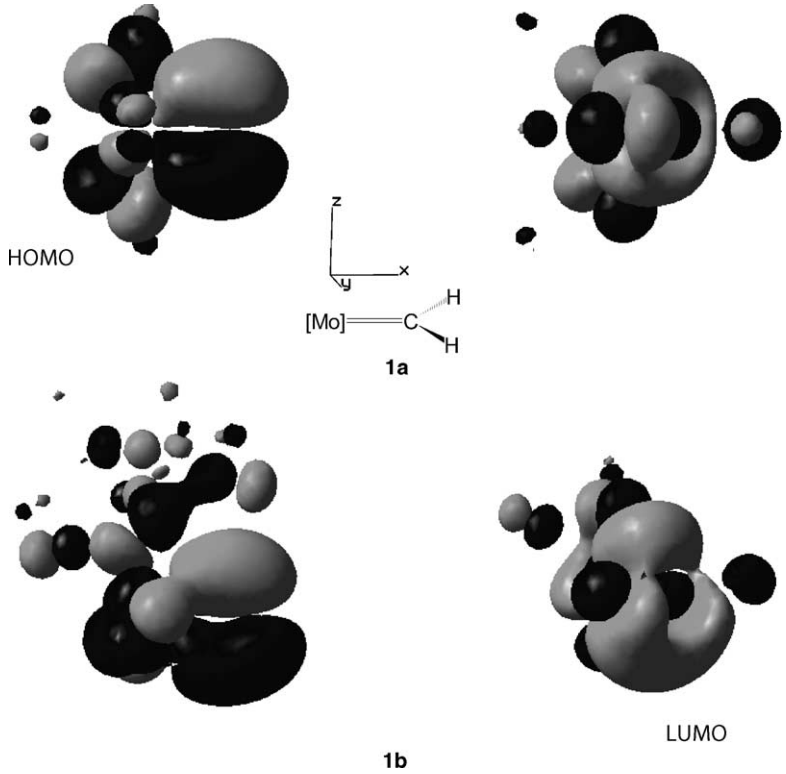

Fig. 4. Isosurfaces of the considered donor (left side) and acceptor (right side) molecular orbitals of the Mo-methylidene centres **1a** and **1b**.

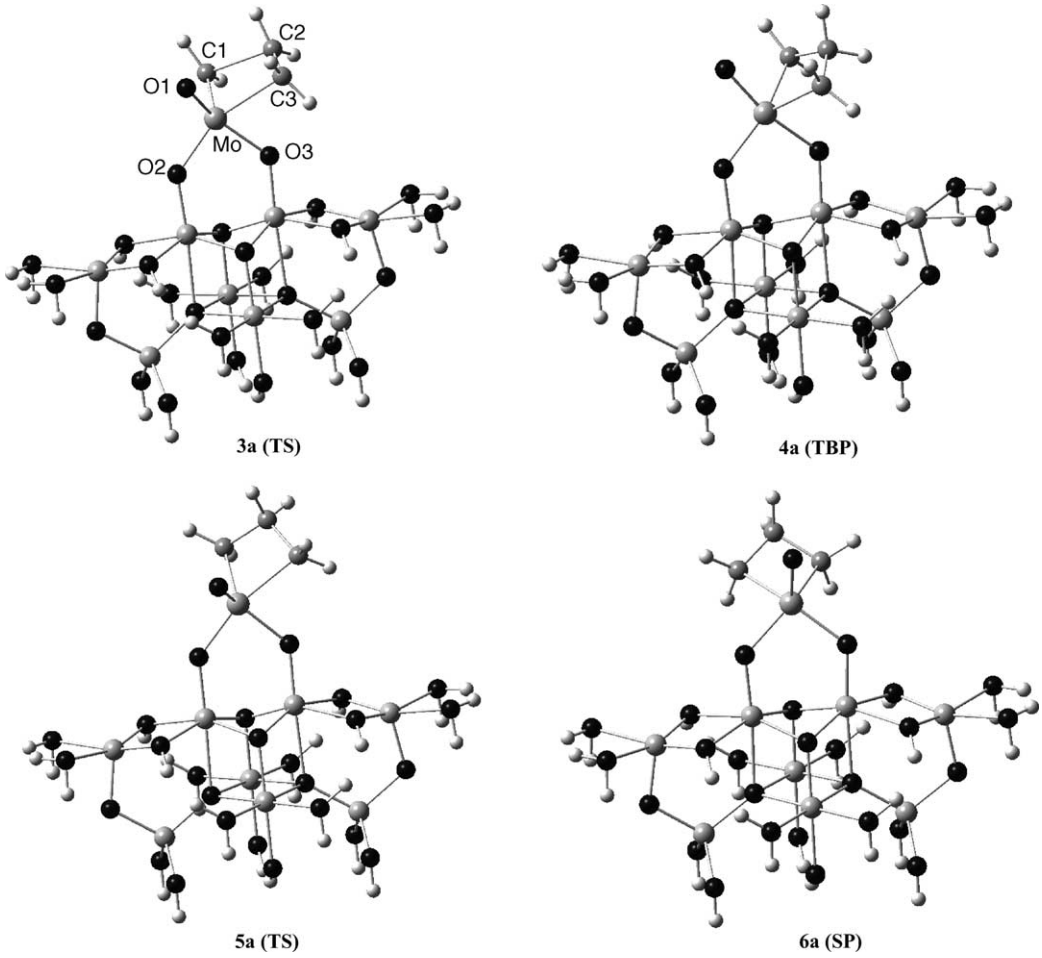

Fig. 5. The minima (**4a**, **6a**) and the transition states (**3a**, **5a**) involved in the pathway of ethene metathesis on the Mo-methylidene centre **1a**.

for **1a** is 6.6 eV. Thus, a nucleophilic attack of ethene on Mo centre is easier in the case of **1b**, comparing to **1a**.

3.3. Ethene metathesis on the Mo-methylidene centres

In Fig. 5, the localised minima and transition states involved in ethene metathesis proceeding on the **1a** centre are depicted, whereas the energy diagram for the overall process is presented in Fig. 6. The structures and energies

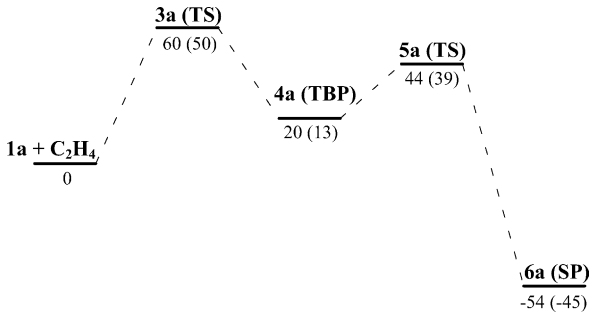

Fig. 6. Energy diagram of ethene metathesis on the Mo-methylidene centre **1a**. The relative energies (kJ mol^{-1}) are obtained from the B3LYP/B// B3LYP/A and B3LYP/A (in parentheses) calculations.

concerning the pathway of ethene metathesis on **1b** are shown in Figs. 7 and 8, respectively.

In both cases, the TBP molybdacyclobutane intermediates (**4a**, **4b**, Figs. 5 and 7) are formed after ethene addition to the carbene bond, in accordance with other reported results [12,14–19]. However, only in the second case, the ethene-molybdenamethylidene π-complex (**2b**) has been localised at the early stage of the reaction. Its formation is moderately exothermic (Fig. 8). As can be seen from Fig. 7 and Table 4, both ethene carbons are weakly bonded to the molybdenum atom, whereas the C1–C2 bond is not formed (0.09 bond order). According to both population analysis methods applied, the Mo charge in the π-complex is decreased by ca. 0.2*e*, comparing to **1b** (Table 3). The C1 atom in **2b** is less negative than the corresponding one in the Mo-methylidene complex **1b**, but the charge difference is smaller than that for the molybdenum. The values from the last row of Table 3 indicate that a charge transfer from the ethene part to the rest of the system takes place (0.22 and 0.12*e*, according to the Mulliken and natural analysis, respectively). These results suggest that the interaction between the HOMO of ethene and the LUMO of **1b** (Fig. 4) plays main role in formation of the π-complex. The energy gap between the corresponding

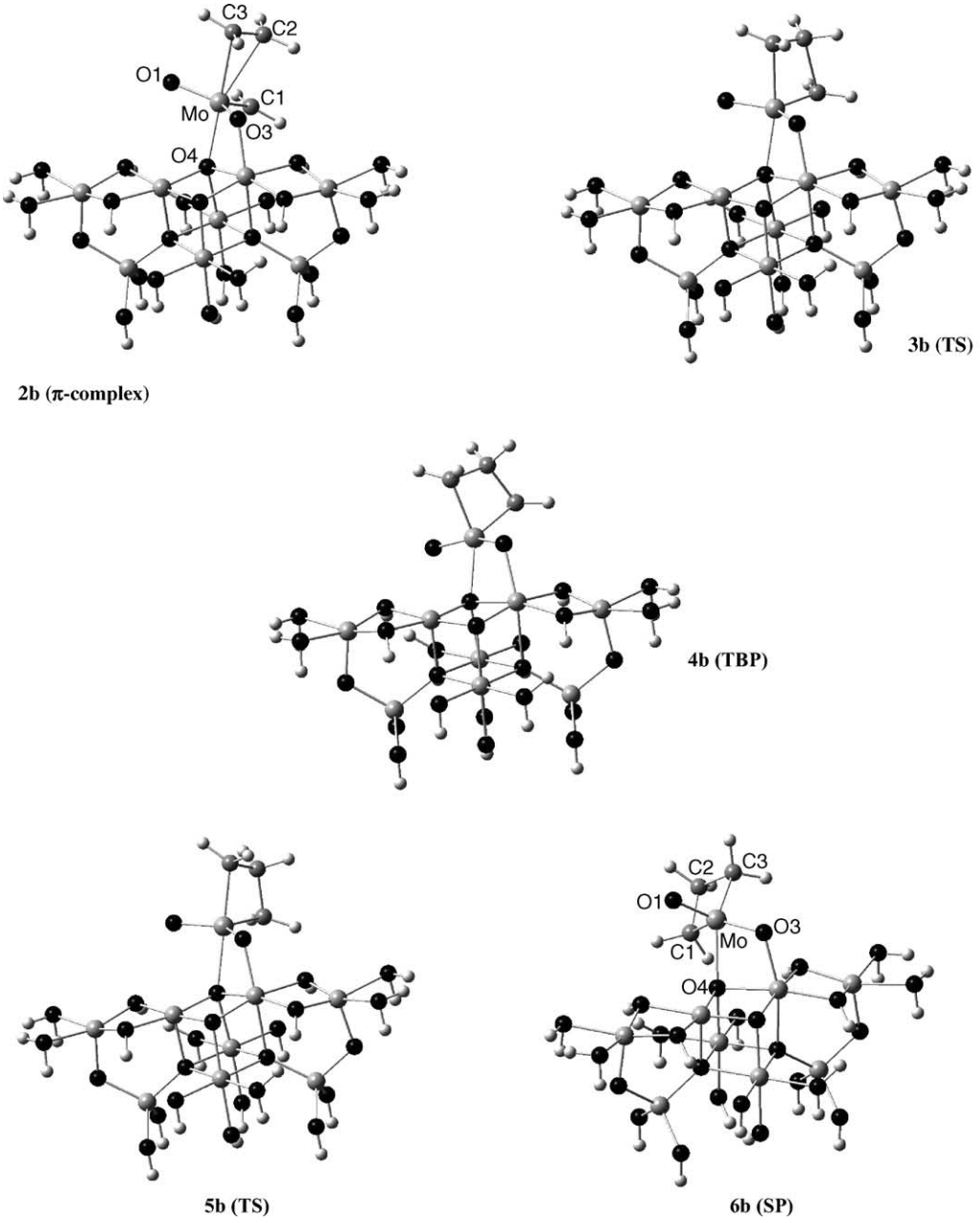

Fig. 7. The minima (**2b**, **4b**, **6b**) and the transition states (**3b**, **5b**) involved in the pathway of ethene metathesis on the Mo-methylidene centre **1b**.

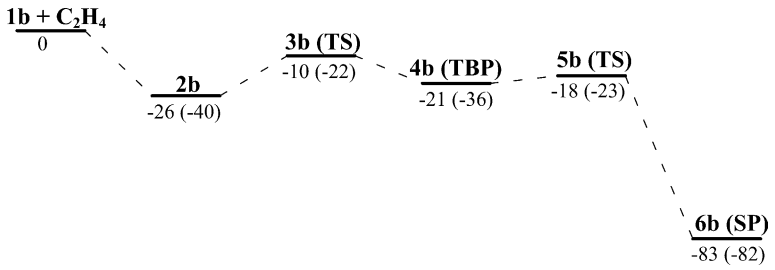

Fig. 8. Energy diagram of ethene metathesis on the Mo-methylidene centre **1b**. The relative energies (kJ mol^{-1}) are obtained from the B3LYP/B//B3LYP/A and B3LYP/A (in parentheses) calculations.

Table 4
Selected atomic distances and bond orders (P) for the π-complex, the TBP molybdacyclobutane intermediates and the corresponding transition states

	3a		**4a**		**2b**		**3b**		**4b**	
	Atomic distance (Å)	P	Atomic distance (Å)	P	Atomic distance (Å)	P	Atomic distance (Å)	P	Atomic distance (Å)	P
Mo–C1	1.955	1.29	2.095	0.92	1.929	1.45	1.957	1.12	2.038	0.90
Mo–C2	2.544	0.24	2.416	0.16	2.585	0.32	2.418	0.31	2.365	0.20
Mo–C3	2.361	0.55	2.094	0.93	2.517	0.36	2.221	0.70	2.071	0.92
C1–C2	2.268	0.36	1.612	0.86	2.898	0.09	2.084	0.46	1.631	0.82
C2–C3	1.421	1.30	1.612	0.86	1.378	1.52	1.45	1.12	1.608	0.86

molecular orbitals in **1a** is 2.2 eV higher, what can explain why the π-complex is not formed in this case.

The π-complex **2b** can rearrange to the TBP molybdacyclobutane (**4b**) via a transition state **3b** (Fig. 7). Both Mo–C3 and C1–C2 bond formations can be clearly noticed in the transition structure (Table 4), however, the latter bond is formed to a less extent. The Mo–C2 interaction is also still noticeable. The Mo–C3 bond order was increased by 0.34 after rearrangement of **2b** to **3b** and following transformation of **3b** to **4b** results in its further increasing by 0.22. As concerns the C1–C2 bond formation, the increment of the bond order from the reactant to the TS (0.37) is close to that from the TS to the product (0.36). Taking into consideration the broken bonds, one can notice that the Mo–C1 bond order is reduced by 0.33, when moving from **2b** to **3b** and further rearrangement to **4b** results in the bond order decrease by 0.22. The corresponding differences for the C2–C3 bond are 0.40 and 0.26, respectively. What is more, the orders of both Mo–C1 and C2–C3 bonds in the transition state **3b** are hardly higher than 1 (Table 4). Based on these results, one can conclude that **3b** is rather a product-like transition state. This is consistent with the fact that formation of the TBP molybdacyclobutane (**4b**) from the π-complex **2b** is a slightly endothermic process (Fig. 8). However, the predicted activation barrier of this step is very low, below 20 kJ mol^{-1} and the overall formation of the TBP intermediate **4b** from the Mo-methylidene (**1b**) and ethene is exothermic.

For comparison, one can consider the **3a** transition state, leading to the TBP molybdacyclobutane intermediate **4a** (Fig. 5). In this case, the predicted activation energy is quite high (60 kJ mol^{-1}, according to the B3LYP/B//B3LYP/A calculations) and the step is clearly endothermic (Fig. 6). The geometry of the transition structure is very similar to that previously described [19], involved in propene metathesis on the (1 0 0) surface of γ-alumina. Thus, it is not considered in detail here. Analogously to **3b**, the formation of the C1–C2 bond in **3a** falls behind the Mo–C3 bond formation (Table 4). This result is also consistent with other reported findings [12,19].

In the transition state **3b**, the total charge transfer from the ethene part to the rest of the system is reduced, comparing to the π-complex **2b** (0.09 and 0.07, according to the Mulliken and natural analysis, respectively). In the case of the **3a** structure, this total charge transfer is even smaller, if any (0.07 and 0.01e, respectively). This indicates that the interaction between the HOMO of ethene and the respective acceptor orbital of the Mo-methylidene site is followed by back donation from the donor orbital of the Mo-methylidene to the LUMO of ethene. The latter effect is mainly responsible for the C1–C2 bond formation.

To continue the catalytic cycle of ethene metathesis, the TBP intermediate must decompose to the [Mo]=C3H$_2$ centre and C1H$_2$=C2H$_2$. However, in the case of the pathway a, this step is identical with the reverse decomposition: **4a** → **1a** + C$_2$H$_4$, because of the C_s symmetry of the TBP intermediate. As concerns the pathway b, the molybdacyclobutane ring in **4b** is also not very unsymmetrical (Table 4), so energetics of its decomposition to [Mo]=C3H$_2$ should be similar to that for the reaction: **4b** → **2b** → **1b** + C$_2$H$_4$. Therefore, the additional calculations were not performed.

Analogously as in the previous works [16–19], the SP molybdacyclobutanes (**6a**, **6b**, Figs. 5 and 7) and the corresponding transition structures (**5a**, **5b**), connecting the respective TBP and SP intermediates, have been localised. The selected atomic distances for the structures are listed in Table 5. As one can see, the geometry of the molybdacyclobutane rings for the corresponding structures in pathways a and b does not differ significantly. The structures of analogous SP molybdacyclobutanes and the transition states involved, as well as the details of the BP → SP rearrangement, were discussed previously [16,17]. For both presently considered pathways, this rearrangement is clearly exothermic, by −74 and −62 kJ mol^{-1}, respectively (B3LYP/B//B3LYP/A, Figs. 6 and 8). The predicted activation barrier for the step **4a** → **6a** is below 30 kJ mol^{-1} (Fig. 6), while the transformation **4b** → **6b** proceeds much more easily (Fig. 8). It should be emphasised that the formation of the SP intermediate is a competitive step to the breakdown of the TBP molybdacyclobutane to the Mo-methylidene site

Table 5
Selected atomic distances (Å) for the SP molybdacyclobutane intermediates and the corresponding transition states

	5a	**6a**	**5b**	**6b**
Mo–C1	2.081	2.200	2.021	2.173
Mo–C2	2.590	2.828	2.338	2.723
Mo–C3	2.204	2.200	2.092	2.121
C1–C2	1.602	1.540	1.671	1.544
C2–C3	1.562	1.540	1.594	1.563

and ethene. Therefore, the former step is undesired, but according to the present results (Figs. 6 and 8), it proceeds easier than the latter one. Because the SP intermediate is much more stable than the TBP one, most of the Mo sites during the process are expected to be present as the less active SP molybdacyclobutane structures.

Thus, both the TBP and SP molybdacyclobutane intermediates play a role in mechanism of alkene metathesis proceeding on the considered Mo-methylidene centres located on the (1 0 0) surface of γ-Al_2O_3. This conclusion is in accordance with the previous findings [16–19]. The present results clearly indicate that the activity of the Mo centre is significantly influenced by its location on the support. It is predicted that the Mo-methylidene centre **1a** is not very reactive towards ethene, because the formation of the TBP intermediate is endothermic and has a relatively high activation barrier (Fig. 6). On the other hand, addition of ethene to **1b** is moderately exothermic and proceeds via the π-complex intermediate (Fig. 8). The latter is a little more stable than the TBP molybdacyclobutane, however, both can rearrange each other with a low activation barrier. Decomposition of the π-complex to **1b** and ethene also occurs easily. Thus, in the light of the present calculations, the overall process of ethene metathesis on **1b** has low energy barriers and can take place at room temperature, in accordance with the experiment [1,6,7,25,43]. The much higher metathesis activity of the **1b** centre, comparing to the **1a** one, is explained by the fact that the support part of the system is more electron withdrawing in the former case. What is more, the carbene bond in **1b** is better exposed to alkene attack. On the other hand, for both considered pathways of ethene metathesis, it is predicted that most of the surface Mo sites reacting with ethene convert further into the SP intermediates that exhibit low activity.

4. Conclusions

Two pathways of ethene metathesis proceeding on Mo-methylidene sites differently located on the (1 0 0) surface of γ-Al_2O_3 have been compared. Alumina has been represented by a relatively large cluster model. In the first case, the Mo-methylidene centre replaced two terminal basic hydroxyl groups attached to the octahedral coordinated aluminium atoms. According to the present calculations, ethene addition to this centre, leading to the trigonal bipyramidal molybdacyclobutane intermediate, is endothermic with a relatively high activation barrier. In the second case, one basic OH group is replaced by the Mo-methylidene moiety but the molybdenum is also directly connected to a bridge oxygen atom of the surface. Such location results in reduced electron density on the active site. This, together with the more suitable geometry of the centre, facilitates alkene addition. Consequently, a stable ethene-molybdenamethylidene π-complex is formed, which can further rearrange with a low energy barrier to the trigonal bipyramidal molybdacyclobutane.

For both pathways investigated, the undesired transformation of the trigonal bipyramidal intermediate to the much more stable square pyramidal one occurs easier than the decomposition of the former to the Mo-methylidene centre and ethene.

Acknowledgments

This work was supported by Polish State Committee for Scientific Research (Grant No. 4 T09A 05623). Computing resources from Academic Computer Centre CYFRONET AGH (SGI Origin 2800 computer, Grant No. KBN/SGI_ORIGIN_2000/PK/109/1999) are gratefully acknowledged.

References

[1] K.J. Ivin, J.C. Mol, Olefin Metathesis and Metathesis Polymerization, Academic Press, London, 1997.
[2] J.C. Mol, Catal. Today 51 (1999) 289.
[3] X. Xu, J.C. Mol, C. Boelhouwer, J. Chem. Soc., Faraday Trans. 1 82 (1986) 2707.
[4] M. Sibeijn, J.A.R. van Veen, A. Bliek, J.A. Moulijn, J. Catal. 145 (1994) 416.
[5] P. Maksimowski, W. Skupiński, J. Mol. Catal. 65 (1991) 187.
[6] H. Aritani, O. Fukuda, T. Yamamoto, T. Tanaka, S. Imamura, Chem. Lett. (2000) 66.
[7] J. Handzlik, J. Ogonowski, E. Sikora, O. Vogt, Przem. Chem. 81 (2002) 184.
[8] A.K. Rappé, W.A. Goddard III, J. Am. Chem. Soc. 104 (1982) 448.
[9] E.V. Anslyn, W.A. Goddard III, Organometallics 8 (1989) 1550.
[10] E. Folga, T. Ziegler, Organometallics 12 (1993) 325.
[11] H.H. Fox, M.H. Schofield, R.R. Schrock, Organometallics 13 (1994) 2804.
[12] Y.-D. Wu, Z.-H. Peng, J. Am. Chem. Soc. 119 (1997) 8043.
[13] K. Monteyne, T. Ziegler, Organometallics 17 (1998) 5901.
[14] Y.-D. Wu, Z.-H. Peng, Inorg. Chim. Acta 345 (2003) 241.
[15] J. Handzlik, J. Ogonowski, J. Mol. Catal. A 175 (2001) 215.
[16] J. Handzlik, J. Ogonowski, J. Mol. Catal. A 184 (2002) 371.
[17] J. Handzlik, J. Catal. 220 (2003) 23.
[18] J. Handzlik, J. Mol. Catal. A 218 (2004) 91.
[19] J. Handzlik, Surf. Sci. 562 (2004) 101.
[20] J.-L. Hérisson, Y. Chauvin, Makromol. Chem. 141 (1971) 161.
[21] R.R. Schrock, J.S. Murdzek, G.C. Bazan, J. Robbins, M. DiMare, M. O'Regan, J. Am. Chem. Soc. 112 (1990) 3875.
[22] G.C. Bazan, E. Khosravi, R.R. Schrock, W.J. Feast, V.C. Gibson, M.B. O'Regan, J.K. Thomas, W.M. Davis, J. Am. Chem. Soc. 112 (1990) 8378.
[23] G.C. Bazan, J.H. Oskam, H.-N. Cho, L.Y. Park, R.R. Schrock, J. Am. Chem. Soc. 113 (1991) 6899.
[24] A. Hu, K.M. Neyman, M. Staufer, T. Belling, B.C. Gates, N. Rösch, J. Am. Chem. Soc. 121 (1999) 4522.
[25] Y. Iwasawa, H. Kubo, H. Hamamura, J. Mol. Catal. 28 (1985) 191.
[26] K.A. Vikulov, I.V. Elev, B.N. Shelimov, V.B. Kazansky, J. Mol. Catal. 55 (1989) 126.
[27] M. Anpo, M. Kondo, Y. Kubokawa, C. Louis, M. Che, J. Chem. Soc., Faraday Trans. 1 84 (1988) 2771.
[28] M. Witko, K. Hermann, R. Tokarz, Catal. Today 50 (1999) 553.
[29] K. Hermann, M. Witko, in: D.P. Woodruff (Ed.), Oxide Surfaces, Elsevier, 2001, (Chapter 4).

[30] R.M. Lambert, G. Pacchioni (Eds.), Chemisorption and Reactivity on Supported Clusters and Thin Films: Towards an Understanding of Microscopic Processes in Catalysis, NATO ASI Series E, vol. 331, Kluwer, Dordrecht, 1997.
[31] R.-S. Zhou, R.L. Snyder, Acta Cryst. B47 (1991) 617.
[32] M.-H. Lee, C.-F. Cheng, V. Heine, J. Klinowski, Chem. Phys. Lett. 265 (1997) 673.
[33] C. Pecharromán, I. Sobrados, J.E. Iglesias, T. González-Carreño, J. Sanz, J. Phys. Chem. B 103 (1999) 6160.
[34] F.H. Streitz, J.W. Mintmire, Phys. Rev. B 60 (1999) 773.
[35] G. Gutiérrez, A. Taga, B. Johansson, Phys. Rev. B 65 (2001) 012101.
[36] K. Sohlberg, S.J. Pennycook, S.T. Pantelides, J. Am. Chem. Soc. 121 (1999) 10999.
[37] D.A. De Vito, F. Gilardoni, L. Kiwi-Minsker, P.-Y. Morgantini, S. Porchet, A. Renken, J. Weber, J. Mol. Struct. (Theochem.) 469 (1999) 7.
[38] J. Räty, M. Suvanto, P. Hirva, T.A. Pakkanen, Surf. Sci. 492 (2001) 243.
[39] O. Maresca, A. Ionescu, A. Allouche, J.P. Aycard, M. Rajzmann, F. Hutschka, J. Mol. Struct. (Theochem.) 620 (2003) 119.
[40] S. Cai, K. Sohlberg, J. Mol. Catal. A 193 (2003) 157.
[41] H. Knözinger, P. Ratnasamy, Catal. Rev. -Sci. Eng. 17 (1978) 31.
[42] L.J. Alvarez, J.F. Sanz, M.J. Capitan, M.A. Centeno, J.A. Odriozola, J. Chem. Soc., Faraday Trans. 89 (1993) 3623.
[43] J. Handzlik, J. Ogonowski, Catal. Lett. 88 (2003) 119.
[44] R.S. Mulliken, J. Chem. Phys. 23 (1955) 1833, 1841, 2338, 2343.
[45] I. Mayer, Chem. Phys. Lett. 97 (1983) 270.
[46] J.P. Perdew, K. Burke, M. Ernzerhof, Phys. Rev. Lett. 77 (1996) 3865.
[47] M.J. Frisch, G.W. Trucks, H.B. Schlegel, G.E. Scuseria, M.A. Robb, J.R. Cheeseman, J.A. Montgomery Jr., T. Vreven, K.N. Kudin, J.C. Burant, J.M. Millam, S.S. Iyengar, J. Tomasi, V. Barone, B. Mennucci, M. Cossi, G. Scalmani, N. Rega, G.A. Petersson, H. Nakatsuji, M. Hada, M. Ehara, K. Toyota, R. Fukuda, J. Hasegawa, M. Ishida, T. Nakajima, Y. Honda, O. Kitao, H. Nakai, M. Klene, X. Li, J.E. Knox, H.P. Hratchian, J.B. Cross, C. Adamo, J. Jaramillo, R. Gomperts, R.E. Stratmann, O. Yazyev, A.J. Austin, R. Cammi, C. Pomelli, J.W. Ochterski, P.Y. Ayala, K. Morokuma, G.A. Voth, P. Salvador, J.J. Dannenberg, V.G. Zakrzewski, S. Dapprich, A.D. Daniels, M.C. Strain, O. Farkas, D.K. Malick, A.D. Rabuck, K. Raghavachari, J.B. Foresman, J.V. Ortiz, Q. Cui, A.G. Baboul, S. Clifford, J. Cioslowski, B.B. Stefanov, G. Liu, A. Liashenko, P. Piskorz, I. Komaromi, R.L. Martin, D.J. Fox, T. Keith, M.A. Al-Laham, C.Y. Peng, A. Nanayakkara, M. Challacombe, P.M.W. Gill, B. Johnson, W. Chen, M.W. Wong, C. Gonzalez, J.A. Pople, Gaussian 03, revision B.03, Gaussian, Inc., Pittsburgh PA, 2003.
[48] A.D. Becke, J. Chem. Phys. 98 (1993) 5648.
[49] P.J. Stevens, J.F. Devlin, C.F. Chabalowski, M.J. Frisch, J. Phys. Chem. 98 (1994) 11623.
[50] P.J. Hay, W.R. Wadt, J. Chem. Phys. 82 (1985) 299.
[51] T.H. Dunning Jr., P.J. Hay, in: H.F. Schaefer, III (Ed.), Modern Theoretical Chemistry, vol. 3, Plenum Press, New York, 1976, p. 1.
[52] C. Peng, P.Y. Ayala, H.B. Schlegel, M.J. Frisch, J. Comp. Chem. 17 (1996) 49.
[53] A.E. Reed, L.A. Curtiss, F. Weinholt, Chem. Rev. 88 (1988) 899.
[54] E.D. Glendening, A.E. Reed, J.E. Carpenter, F. Weinhold, NBO Version 3.1.